

Modeling of a twisted-Kagome HoAgGe spin ice using Reduced-Configuration-Space Search and Density Functional Theory

Gunnar F. Schwertfeger, Po-Hao Chang, Predrag Nikolić, and Igor I. Mazin

*Department of Physics and Astronomy, George Mason University, Fairfax, VA 22030, USA and
Quantum Science and Engineering Center, George Mason University, Fairfax, VA 22030, USA*

The Kagome lattice is a 2D network of corner sharing triangles found in several rare earth materials resulting in a complicated and often frustrated magnetic system. In the last decades, modifications of the motif, such as breathing Kagome, asymmetric Kagome, and twisted Kagome were brought into the limelight. In particular, the latter has lower symmetry than the original Kagome and thus allows implementations of an “Ising-local” Hamiltonian, leading to a 2D spin ice. One such material implementation, HoAgGe, was recently reported to have an exceptionally rich phase diagram and is a strongly frustrated 2D spin-ice material with a twisted-Kagome geometry. In the presence of an external magnetic field the compound exhibits step-like magnetization plateaus at simple fractions of the saturation magnetization. It is believed that this phenomenon results from strong single-site anisotropy, which in HoAgGe was found to be in-plane and along a high-symmetry direction. Previous Monte Carlo simulations with empirical exchange parameters explain some, but not all experimental observations. In this work we present (a) first-principle calculations of the crucial model parameters and (b) direct energy minimization via a Reduced-Configuration-Space search, as well as Monte-Carlo simulations of the field-dependent phase diagram. We find that for HoAgGe the calculated exchange parameters are very different from the earlier suggested empirical ones, and describe the phase diagram much more accurately. This is likely because the first-principles parameters are, in addition to geometrically, also parametrically frustrated.

I. INTRODUCTION

Magnetic frustration has been the source of many exotic phenomena in matter. In 3D rare-earth pyrochlore compounds, for instance, one finds a rather unique phenomenon dubbed “spin ice” [1]. In a new twist, a 2D material, HoAgGe, was recently reported[2] to be an example of 2D spin ice. Spin ice is, typically, a highly frustrated magnetic system where each magnetic site has a strong uniaxial anisotropy, with the axis varying from site to site according to the crystal symmetry.

The kagome lattice is formed from corner sharing equilateral triangles (Fig. 1). As the kagome lattice is the 2D analogue of the 3D pyrochlore lattice, it is natural to look for spin ice behavior there. In the last decades, various interesting modifications of the kagome lattice have also been discussed in the literature, such as breathing kagome[3], distorted kagome[4], square kagome[5] etc. One of the newest developments is the so-called[6] twisted Kagome lattice, where the alternating triangles in the lattice are twisted around their centers in the opposite directions. This operation lowers the symmetry from $P6/mmm$ to $P6/2m$. In particular, the site symmetry is lowered from mmm to $m2m$, as one can see from Fig. 1, and the global inversion symmetry is also lost.

The recently reported magnetic compound, HoAgGe[2] has this twisted kagome structure, with the twisting angle $\sim 15.6^\circ$ (again as depicted in Fig. 1). Ho^{3+} atoms in this compound have 10 f-electrons, a large orbital moment and strong spin-orbit coupling. Therefore, the single-site anisotropy is large and, generally speaking, can have any easy axis, in or out of plane[7]. Experimental evidence suggests that the easy axis for Ho is along a high-symmetry direction as indicated by the arrows in

Fig. 1. Our first-principle calculations described below confirm this.

In this case, the magnetic Hamiltonian, to a good approximation, is local-Ising, in the sense that each spin can assume only two directions. This results in a “two-in-one-out” spin-ice rule in plane for the triangular nearest neighbor interactions between Ho atoms in the twisted kagome lattice. This is analogous to the “two-in-two-out” rule observed in the tetrahedra in pyrochlore spin-ice compounds [1]. Existing experimental data are reasonably well consistent with this picture[2, 8] (albeit small, but distinct deviations from the infinite-anisotropy model were reported in Ref. [8]). As the dominant interaction is antiferromagnetic, the ground state in zero field has zero magnetization, and the spins form a $\sqrt{3} \times \sqrt{3}$ supercell, as depicted in Fig. 7, with the magnetic space group retaining the hexagonal symmetry, $P6'm2'$. In the in-plane saturation field, whose value depends on the field direction, all spins assume the direction most parallel to the applied field,

Experimentally, the “iceness” of the system is reflected in the multiple magnetization steps in an in-plane magnetic field \mathbf{h} . Indeed, HoAgGe exhibits, in an external magnetic field, several of these unique magnetic steps. These steps are simple fractions of the total magnetization. While some of the larger steps (such as the 1/3 and 2/3 magnetization plateaus observed for $\mathbf{h}||y$) have been explained in earlier works [2], many smaller magnetization steps, particularly those observed for $\mathbf{h}||x$, have not been explained.

To this end, we have, first, performed first-principles DFT+U calculations, making sure that the Hund’s rule on Ho is respected[7, 9], as discussed below, and extracted six Heisenberg exchange parameters, up to the

5th nearest neighbors (as opposed to three parameters used in the empirical model of Ref. [2]). The resulting parameters are completely different from latter, yet provide a better description of experimentally observed plateaus not only for $\mathbf{h}||y$, but also for $\mathbf{h}||x$. Using these parameters, we constructed full exchange Hamiltonians (as discussed below, the Dzyaloshinskii-Moriya and dipole-dipole interactions appear to be not important), and directly minimized the energy by performing a search over a Reduced-Configuration-Space for all possible supercells up to 18 formula units and constructed the zero-temperature phase diagram for both field directions. We found that all major phases are very stable, and secondary phases, corresponding to smaller magnetization plateaus, are on the borderline of stability, but still present. Thus, we identified all 10 experimentally observed phases.

In addition, we attempted Monte-Carlo simulations similar to those in Ref. [2], but, as opposed to their model, our calculated Hamiltonian is much more frustrated, so finding the global energy minimum in MC calculations is challenging.

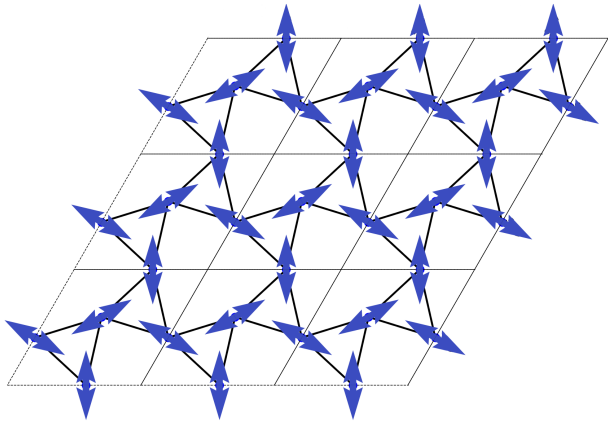


FIG. 1: Twisted Kagome Lattice with J_1 bonds visualized (a 3×3 supercell is shown). The arrows indicate the easy axis in HoAgGe.

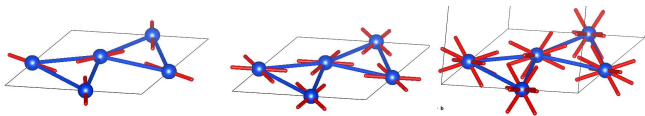


FIG. 2: Possible spin models on a twisted kagome lattice with a strong easy axis. Left: Ising-ice model (same as Fig. 1). Center: 4-Potts-ice model. Right: 8-Potts-ice model. The red rods indicate the hypothetical easy axes.

II. GENERAL MODEL

A. Crystal Lattice Hamiltonian

The Hamiltonian for the Spin-Ice crystal HoAgGe is:

$$H[M; J_\alpha, h] = - \sum_{\alpha} J_{\alpha} \sum_{\langle i, j \rangle_{\alpha}} \hat{\mathbf{S}}_i \cdot \hat{\mathbf{S}}_j - h \sum_i \hat{\mathbf{S}}_i \cdot \hat{\mathbf{h}}, \quad (1)$$

where $M = \{\hat{\mathbf{S}}_0, \hat{\mathbf{S}}_1, \dots, \hat{\mathbf{S}}_N\}$ defines a particular state of the crystal lattice, J_{α} are Heisenberg exchange parameters and h the applied magnetic field along $\hat{\mathbf{h}}$. All spins, $\hat{\mathbf{S}}_i$ and $\hat{\mathbf{h}}$ are unit length vectors in \mathbb{R}^3 . Here, i, j label lattice sites, and α enumerates the Ho-Ho bonds of different lengths on which two spins interact (shown in Fig. 3). Again, as the Ho atoms have large magnetic moments, we can treat these spins classically. In addition, as the magnetic moments of each Ho atom are either at $2\pi/3$ rad or parallel to all other neighboring moments, the Dzyaloshinskii-Moriya interaction may safely be absorbed into the exchange parameters, J_{α} .

Using a method described in a previous paper by some of us [10], we considered periodic magnetic orders as ground-state candidates, with tessellating supercells of various sizes and shapes. A supercell effectively has periodic boundary conditions; if a supercell is very small, then a long-range exchange parameter doubles back on the same supercell atom, which results in a constant positive addition to the lattice energy per antiferromagnetic pair or a constant negative addition per ferromagnetic pair. However as we search supercells containing up to octodecuple ($\times 18$) Ho atoms, all six exchange parameters play nontrivial roles.

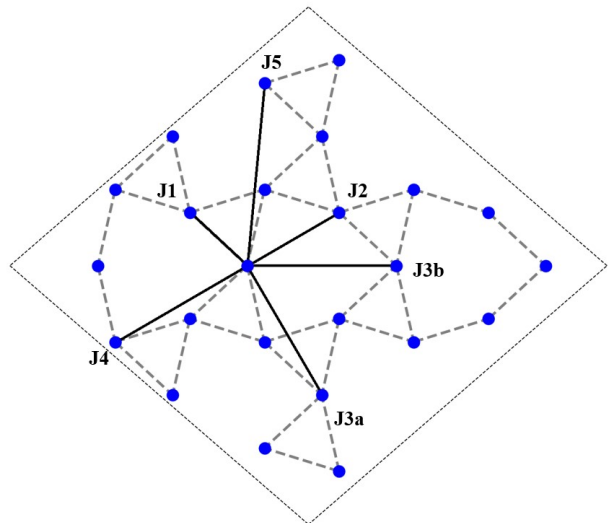


FIG. 3: Nearest neighbor exchange interactions, J_1 to J_5 , depicted for a single atom.

Exchange interactions are defined by their relative distances and crystallographic symmetry. For $J_1, J_2, J_4,$

and J_5 it is enough to use only the corresponding bond lengths to distinguish interaction types. However, for J_3 we have elected to divide these interactions further into crystallographically inequivalent J_{3a} and J_{3b} (in Ref. [2] they were assumed to be equal, however there is no microscopic justification for that).

Atoms joined by J_2 , J_4 , or J_5 couplings also satisfy the two-in-one-out spin-ice rule, further compounding the system's frustration. This is particularly true in the case of J_5 interactions as, like the nearest neighbor J_1 , neighboring J_5 pairs also form corner sharing triangles between atoms. These interactions form decoupled lattices, each still obeying the spin-ice rule between triangles of interacting atoms.

By finding the lattice configurations which minimize Eq. 1 for particular values of J_α and h , the magnetic plateaus observed experimentally should be reproduced given a sufficiently large maximum magnetic unit cell.

For a particular super cell of N atoms, if each atom is in one of q possible states, the total number of configurations of the super cell is simply q^N , meaning the total number of elements in the configuration space, \mathbb{M} , is finite. On sufficiently small lattices with up to $N = 18$ sites, one formally can generate every possible spin configuration and check its energy, but the number of configurations grows exponentially with system size. Using Eq. 1 however, we can greatly reduce the number of states in \mathbb{M} that need to be considered by eliminating symmetrically equivalent states.

For any particular state, $M \in \mathbb{M}$, we define the constants; $C_\alpha[M]$ and $\langle M \rangle_i$ using Eq. 2 and Eq. 3.

$$C_\alpha[M] = \sum_{\langle i,j \rangle_\alpha} \hat{\mathbf{S}}_i \cdot \hat{\mathbf{S}}_j \quad (2)$$

$$\langle M \rangle_i = \sum_j \hat{\mathbf{S}}_j \cdot \hat{\mathbf{e}}_i \quad (3)$$

Using Eq. 1, the Hamiltonian for any given state may be written as Eq. 4.

$$H_M[J_\alpha, h] = - \sum_\alpha J_\alpha C_\alpha - \sum_i h_i \langle M \rangle_i \quad (4)$$

meaning each Hamiltonian for a state in \mathbb{M} can be characterized by $\alpha + 3$ parameters. By collecting only the states which exhibit unique values for C_α and $\langle M \rangle_i$ and therefore by Eq. 4 constitute a unique Hamiltonian, the total number of unique states of the super cell is greatly diminished, and the search over configuration space for the lowest energy state for any combination of J_α and h is significantly reduced. For this reason, we refer to this method as a Reduced-Configuration-Space Search (RCS Search).

B. Magnetic Dipole Interaction

In principle, in rare-earth systems the magnetic dipole-dipole interactions may be relevant; they can be introduced to the Hamiltonian as follows:

$$E_{dd} = - \frac{g_{dd}}{|\mathbf{r}_{ij}|^3} \left(3 \left(\hat{\mathbf{S}}_i \cdot \hat{\mathbf{r}}_{ij} \right) \left(\hat{\mathbf{S}}_j \cdot \hat{\mathbf{r}}_{ij} \right) - \left(\hat{\mathbf{S}}_i \cdot \hat{\mathbf{S}}_j \right) \right)$$

$$g_{dd} = \frac{\mu_0 \mu_B^2 g^2}{4\pi}$$

$$\langle E_{dd} \rangle = \sum_{\alpha, \langle i,j \rangle_\alpha} \frac{\left(3 \left(\hat{\mathbf{S}}_i \cdot \hat{\mathbf{r}}_{ij} \right) \left(\hat{\mathbf{S}}_j \cdot \hat{\mathbf{r}}_{ij} \right) - \left(\hat{\mathbf{S}}_i \cdot \hat{\mathbf{S}}_j \right) \right)}{|\mathbf{r}_{ij}|^3}$$

$$H_M[J_\alpha, h, g_{dd}] = -J_\alpha C_\alpha - h_i \langle M \rangle_i - g_{dd} \langle E_{dd} \rangle \quad (5)$$

An additional term to the Hamiltonian means that each Hamiltonian is now characterized by $\alpha+4$ parameters and when searching through all forms of M in \mathbb{M} some degeneracies may be lifted allowing for more unique Hamiltonians to be observed. For the HoAgGe crystal, however, this appears to be a largely negligible effect.

C. Calculation of exchange parameters

TABLE I: The comparison between the effective exchange coupling constants up to 4th nearest neighbor assumed by Zhao *et al*[2] and up to 5th nearest neighbor calculated using DFT and GF. The values of the former are normalized to $J_1 = 2$ meV and the latter are normalized to $J_1 = 3.154$ meV. NN here is the coordination number of the corresponding bond. Note that in Ref. [2] J_{3a} , J_{3b} and J_4 were assumed to be equal.

		Ref. [2]	DFT-GF
	NN	$J_i/ J_1 $	
J_1	4	1	1
J_2	2	-0.115	-0.442
J_{3a}	4	-0.064	-0.131
J_{3b}	2	-0.064	-0.175
J_4	2	-0.064	-0.023
J_5	4		-0.067

The calculations described below have been, to a large part, described in an earlier paper[8], but we briefly outline them below for completeness. A numerical-orbital-based [11] DFT code OpenMX [12] was first used to obtain the ground state Hamiltonian. The Perdew-Burke-Enzerhof (PBE) [13] generalized gradient approximation was employed to describe exchange-correlation effects. To ensure the proper f-shell occupation, a large Hubbard U correction is used to account for the strongly correlated Ho $4f$ states [14, 15] (since these states are well

removed from the Fermi level, the exact value of U in this case is not important, as compared to d -metals. The exchange coupling constants are then calculated perturbatively using Green's function method [16, 17] implemented in OpenMX 3.9 [18, 19].

III. ANALYSIS OF HoAgGe MODEL

A. Average Magnetization

The minimum antiferromagnetic supercell is the $\sqrt{3} \times \sqrt{3}$ (Fig. 4 Red). Using this supercell and imposing periodic boundary conditions gives a system of nine atoms with each atom in one of the two states. There are then $2^9 = 512$ total elements in the configuration space meaning 512 possible states can be represented on the $\sqrt{3} \times \sqrt{3}$ super cell. However, the number of states with unique Hamiltonians is only 88. These states are then compared to find the lowest energy configuration as the applied magnetic field is increased.

This is done for all possible guesses of magnetic unit cells with the volume less than or equal to six times the volume of a single unit cell. This gives 780 acceptable supercells. The states that exhibit unique Hamiltonians are then compared against each other to create a list of 608101 states with unique Hamiltonians covering 27 possible supercell shapes. Of those, only 8 shapes are appear to be relevant to minimum-energy states for any in-plane field. These shapes are shown in Fig. 4 .

Using the exchange parameters conjectured by Zhao et al [2] and applying the above protocol, the resulting phase diagram can then be directly compared with the experiment in Fig. 5. Note again that there is no distinction between bonds of type J_{3a} and J_{3b} for their set of parameters.

While the resulting magnetization curves (dashed) do represent, to some extent, experimental measurements, specifically, the two most prominent magnetization plateaus at the $1/3$ and $2/3$ magnetizations, this Hamiltonian does not fully describe the experiment.

Using the other set of exchange parameters, calculated, as described, using DFT-GF method, the same states can again be analyzed with new parameters and the total magnetization is plotted in Fig. 6.

Importantly, this set of parameters distinguishes between J_{3a} and J_{3b} while including the further neighbor coupling parameter, J_5 . For this reason, the calculated values of J_α appear significantly different than those found empirically but still describe the system as sufficiently. In fact, these inclusions significantly improve the accuracy of the model, particularly in the X direction, perpendicular to the easy axis of the Ho atoms.

These new parameters exhibit several small steps between the $1/3$ plateau and the fully saturated state. These are the $1/2$, and $3/4$ states. These states were not observed using the empirical parameters. In total, the inclusion of the further nearest neighbor, J_5 , and distin-

guishing between J_{3a} and J_{3b} type interactions resulted in ten distinct magnetization steps[20] again defined by the eight shaped cells shown in Fig. 4. The inclusions of further neighbors does not generate significant change for magnetic fields applied in the Y direction, but still describe the magnetic behavior as accurately as the empirical parameters, even finding the same ground state (Fig. 7).

Surprisingly, what was initially assumed to be a small $1/6$ magnetic plateau is not directly observed using this method. However, a small, near coincident $1/5$ state is observed at the phase boundary between the $0/3$ and $1/3$ states. We now believe the small plateau observed experimentally is actually a $1/5$ state as opposed to the initially theorized $1/6$ state.

Similarly, we also observe a $1/2$ state for fields applied in both the X and Y directions. For the former in particular, this step appears quite prominent. However, by inspecting the average energy per Ho atom of the competing states, it is clear that this $1/2$ state, while broad, is extremely close in energy to the $1/3$ and $2/3$ states, indicating low stability. This is shown directly in Fig. 8 as the competing $\sqrt{3} \times \sqrt{3}$ and $\sqrt{3} \times 3$ cells have a difference in energy less than $6 \mu\text{eV}$ (i.e., 0.07 K in temperature units) for any value of h between the $1/2$ and $2/3$ phase transitions. This energy difference is well within the range of thermal fluctuations to trigger these phase transitions, as well of the accuracy of the model assumptions, such as infinite anisotropy.

Notably, this direct comparison of competing energy states cannot be done easily using a more standard Monte Carlo approach and further demonstrates the utility of this method.

In total, using a RCS Search method, we found the ground state and all major magnetization steps observed in experiment (0 , $1/5(x)$, $1/5(y)$, $1/3(x)$, $1/3(y)$, $2/3(y)$, $3/4(x)$, $3/4(y)$, and $1(x, y)$). Among them, all states previously found empirically in Ref. [2] were again seen and confirmed using this method.

B. $J_\alpha - h$ phase diagrams

Using this procedure, it is relatively simple to vary the parameters, J_α and h , and search for which Hamiltonian of which magnetic unit cell has the lowest energy. By repeating this process and varying any one J_α , phase diagrams of the system's behavior can be produced. As all exchange parameters are normalized to the nearest neighbor one, we calculate the phase diagrams for all interactions other than the first. This allows a visual inspection for the stability against any of these parameters and the behavior of the model. The resulting J_2 phase diagram for a field applied in the X direction is shown in Fig. 9. From inspecting the remaining J_{3a} , J_{3b} , J_4 , and J_5 magnetic phase diagrams[21], for fields applied in the X direction in particular, it is clear that almost no adjustments can easily be made to the internal cou-

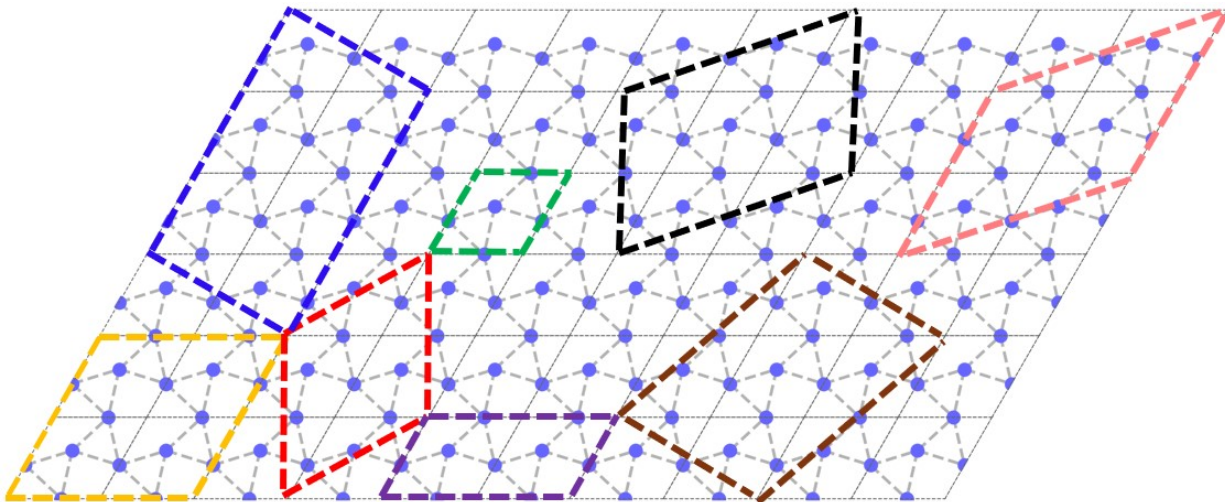


FIG. 4: Magnetic supercells exhibiting the lowest energy for different in-plane fields. The 1×1 Super cell (Green). The 2×1 Super cell (purple). The 2×2 Super cell (Yellow). The $\sqrt{3} \times \sqrt{3}$ Super cell (Red). The $\sqrt{3} \times 2$ Super cell (Pink). The $\sqrt{7} \times \sqrt{3}$ Super cell (Black). The $\sqrt{3} \times \sqrt{7}$ Super cell (Brown). The $\sqrt{3} \times 3$ Super cell (Blue).

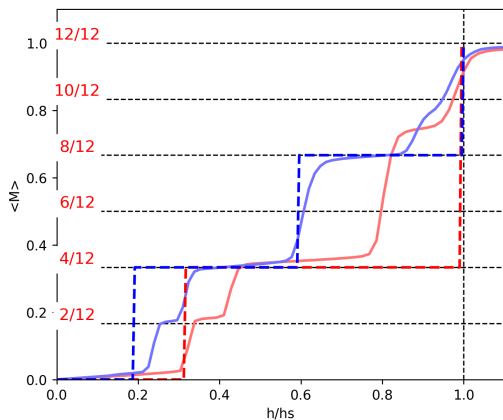


FIG. 5: Average Ho^{3+} magnetization as an external magnetic field is applied perpendicular (X, Red) and parallel (Y, Blue) to the easy axis as found by direct minimization and empirical exchange parameters of Ref. [2] (dashed), compared to experiment[8].

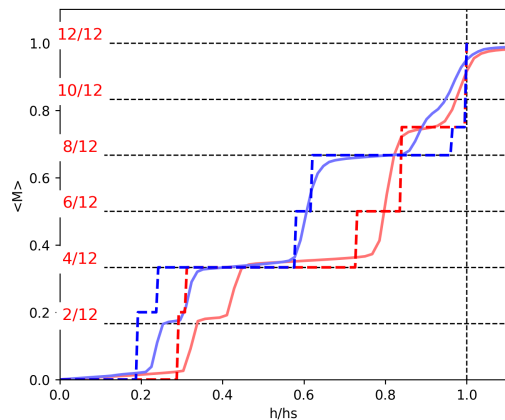


FIG. 6: Average Ho^{3+} magnetization as an external magnetic field is applied perpendicular (X, Red) and parallel (Y, Blue) to the easy axis found using direct minimization and our calculated DFT-GF exchange parameters (dashed) compared to experiment[8].

pling parameters without seriously altering the behavior of the model, in some cases introducing new magnetic plateaus, in others removing steps. This indicates that any further adjustment to the model would likely require either the introduction of further neighbor interactions, new interactions, or a search over a larger RCS.

C. Monte Carlo

Despite being systematic, a direct search of the Reduced-Configuration-Space only applies to zero temperature and is limited in terms of the size of the magnetic unit cell. With this in mind, we have investigated

the phase diagrams using Monte Carlo (MC) simulations. The classical dynamics of our model is adequately addressed with the Metropolis-Hastings algorithm and simulated annealing. The main challenge is that due to high frustration of our DFT-GF Hamiltonian the free energy landscape is crowded with metastable states; we mitigate this by a combination of annealing, aggressive averaging and database bookkeeping of lowest energy states.

These MC simulations were performed on a periodic 18×18 lattice using the same annealing procedure at zero temperature for both the empirically found and the calculated parameters.

MC simulations using the empirical exchange parameters result in clear magnetization steps which again

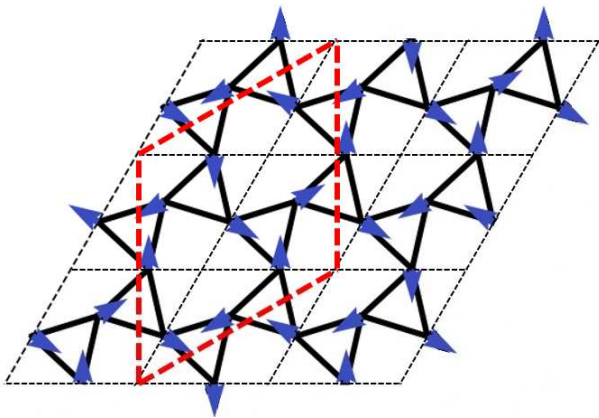


FIG. 7: The ground state $\sqrt{3} \times \sqrt{3}$ supercell (Red) with Magnetic Space Group $P\bar{6}'m2'$

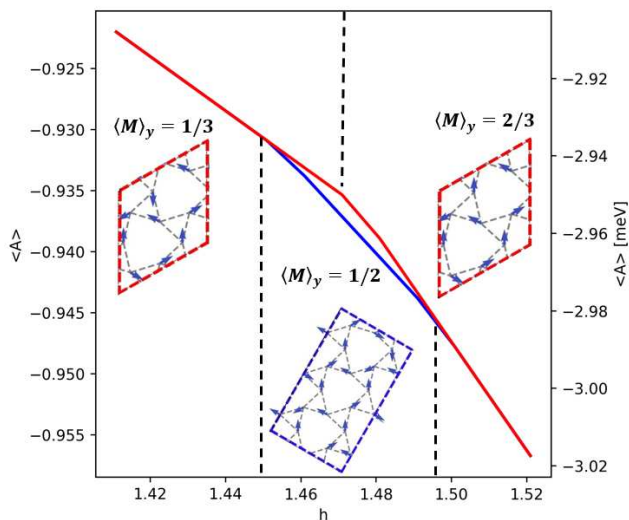


FIG. 8: Minimum average energy per Ho atom ($\langle A \rangle$) of the $\sqrt{3} \times \sqrt{3}$ (Red) and $\sqrt{3} \times 3$ (Blue) Magnetic Unit Cells as an external magnetic field is applied ($h||y$). (Vertical dotted lines indicating phase transitions)

match some, but not all of the steps observed experimentally, and are in agreement with the MC simulation reported in Ref. [2]. When using our first-principles parameters, which include J_5 bonds and distinguishing between J_{3a} and J_{3b} bonds, MC results in a less clear image of the magnetization plateaus, but matches experimental observations far more closely for fields applied in both the X and Y directions[22]. Thus, the first principles parameters pass the test of being relevant in the thermodynamic limit better than the empirical ones.

The noise present in the Monte Carlo simulations performed with our calculated parameters demonstrates how much more frustrated the system becomes with the inclusion of further neighbor interactions. To 'smooth out' this noise would require exceedingly long simulations.

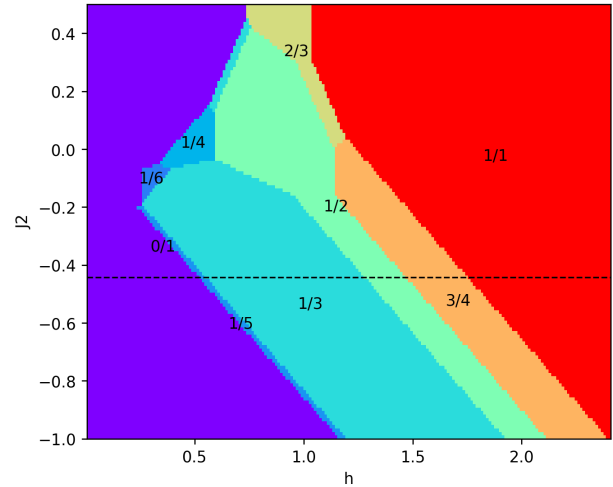


FIG. 9: J_2 Magnetic phase diagram for a magnetic field applied in the X direction. Colors represent average magnetization in the X direction. The dotted line is the theorized value for J_2

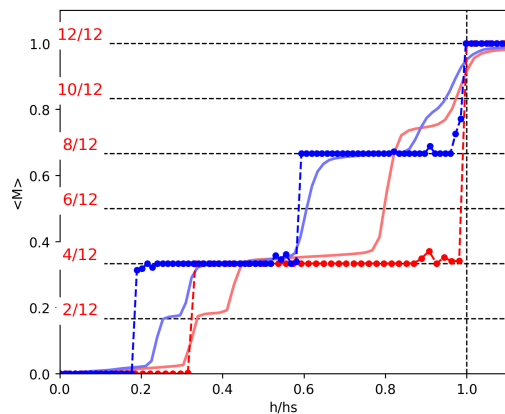


FIG. 10: Monte Carlo simulation of average Ho^{3+} magnetization as an external magnetic field is applied perpendicular (X, Red) and parallel (Y, Blue) to the easy axis calculated using empirical exchange parameters from Ref. [2] (dashed), compared to experiment[8].

IV. CONCLUSIONS

By searching over a Reduced-Configuration-Space for the minimum energy of differently shaped magnetic unit cells of the twisted Kagome lattice and through the use of first principle DFT-GF calculations to determine exchange parameters, we have been able to reproduce the magnetization plateaus observed in experimentation. We have also determined that the employment of larger magnetic unit cells and further neighbor interactions are crucial in reproducing the behavior observed in experiment.

In addition, we have shown the utility of a unique

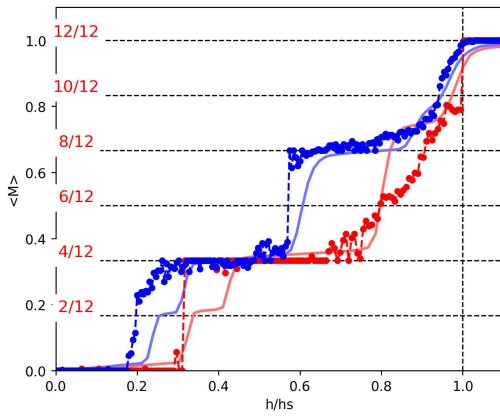


FIG. 11: Monte Carlo simulation of average Ho^{3+} magnetization as an external magnetic field is applied perpendicular (X, Red) and parallel (Y, Blue) to the easy axis calculated using DFT-GF first-principles exchange parameters (dashed), compared to experiment[8].

combination of approaches (DFT-GF and RCS Search method) to a complicated system like HoAgGe twisted Kagome, with advantages over more standard methods. We note that it is possible that the full phase diagram could be better captured using magnetic unit cells larger than six times the single unit cell volume[23]. Other limitations include even longer-range exchange interactions (HoAgGe being a metal, we expect the long range exchange to be of RKKY type, i.e., only cubically decaying) and deviations from the ideal Ising model.

ACKNOWLEDGMENTS

We are grateful to Nirmal Ghimire for attracting our attention to this compound, sharing their experimental data, and for many useful discussions. This work was supported by the Office of Naval Research through grant #N00014-23-1-2480.

-
- [1] A. P. Ramirez, A. Hayashi, R. J. Cava, R. Siddharthan, and B. S. Shastry, Zero-point entropy in ‘spin ice’, *Nature* **399**, 333 (1999).
- [2] K. Zhao, H. Deng, H. Chen, K. A. Ross, V. Petříček, G. Günther, M. Russina, V. Hutanu, and P. Gegenwart, Realization of the kagome spin ice state in a frustrated intermetallic compound, *Science* **367**, 1218 (2020).
- [3] M. Ezawa, Higher-order topological insulators and semimetals on the breathing kagome and pyrochlore lattices, *Phys. Rev. Lett.* **120**, 026801 (2018).
- [4] M. Hering, F. Ferrari, A. Razpopov, I. I. Mazin, R. Valentí, H. O. Jeschke, and J. Reuther, Phase diagram of a distorted kagome antiferromagnet and application to y -kagellasilite, *npj Computational Materials* **8**, 10 (2022).
- [5] J. Richter, J. Schulenburg, P. Tomczak, and P. Schmalfuß, The heisenberg antiferromagnet on the square-kagome lattice, *Condensed Matter Physics* **12**, 10 (2009).
- [6] Y. N. Huang, H. O. Jeschke, and I. I. Mazin, Crrhas: a member of a large family of metallic kagome antiferromagnets, *npj Quantum Materials* **8**, 32 (2023).
- [7] Y. Lee, R. Skomski, X. Wang, P. P. Orth, Y. Ren, B. Kang, A. K. Pathak, A. Kutepov, B. N. Harmon, R. J. McQueeney, I. I. Mazin, and L. Ke, Interplay between magnetism and band topology in the kagome magnets rmn_6sn_6 , *Phys. Rev. B* **108**, 045132 (2023).
- [8] H. Bhandari, P.-H. Chang, R. B. Regmi, B. G. Márkus, L. Forró, J. F. Mitchell, I. I. Mazin, and N. J. Ghimire, Tunable topological transitions in the frustrated magnet hoage, *Communications Materials* **6**, 52 (2025).
- [9] Y. Lee, Z. Ning, R. Flint, R. J. McQueeney, I. I. Mazin, and L. Ke, Toward a first-principles theory of rare-earth ions in crystals (2024), arXiv:2407.10067 [cond-mat.mtrl-sci].
- [10] P.-H. Chang and I. I. Mazin, Exploring metamagnetism in triangular ising networks: Insights from further-neighbor interactions with a case study on erga_2 , *Phys. Rev. B* **110**, 014418 (2024).
- [11] T. Ozaki, Variationally optimized atomic orbitals for large-scale electronic structures, *Phys. Rev. B* **67**, 155108 (2003).
- [12] OpenMX, The code OPENMX pseudoatomic basis functions, and pseudopotentials are available under terms of the GNU-GPL on a web site, <http://www.openmx-square.org/>.
- [13] J. P. Perdew, K. Burke, and M. Ernzerhof, Generalized Gradient Approximation Made Simple, *Phys. Rev. Lett.* **77**, 3865 (1996).
- [14] A. I. Liechtenstein, V. I. Anisimov, and J. Zaanen, Density-functional theory and strong interactions: Orbital ordering in Mott-Hubbard insulators, *Physical Review B* **52**, R5467 (1995).
- [15] S. L. Dudarev, G. A. Botton, S. Y. Savrasov, C. J. Humphreys, and A. P. Sutton, Electron-energy-loss spectra and the structural stability of nickel oxide: An LSDA+U study, *Physical Review B* **57**, 1505 (1998).
- [16] V. Antropov, M. Katsnelson, and A. Liechtenstein, Exchange interactions in magnets, *Physica B: Condensed Matter* **237–238**, 336 (1997).
- [17] M. I. Katsnelson and A. I. Liechtenstein, First-principles calculations of magnetic interactions in correlated systems, *Physical Review B* **61**, 8906 (2000).
- [18] A. Terasawa, M. Matsumoto, T. Ozaki, and Y. Gohda, Efficient Algorithm Based on Liechtenstein Method for Computing Exchange Coupling Constants Using Localized Basis Set, *Journal of the Physical Society of Japan* **88**, 114706 (2019).
- [19] M. J. Han, T. Ozaki, and J. Yu, Electronic structure, magnetic interactions, and the role of ligands in mn_n ($n = 4, 12$) single-molecule magnets, *Phys. Rev. B* **70**, 184421 (2004).
- [20] These are the $0/1$, $1/5(x)$, $1/5(y)$, $1/3(x)$, $1/3(y)$, $1/2(x)$, $2/3(y)$, $3/4(x)$, and $1/1(x)$, $1/1(y)$ magnetization plateaus observed.
- [21] J_{3a} , J_{3b} , J_4 , J_5 phase diagrams not shown here but follow

similar trends to the J_2 phase diagram.

- [22] All Monte Carlo simulations across the different parameter sets were performed using the same simulation protocol.
- [23] This was later confirmed using the GMU Cluster computer, HOPPER, for magnetic unit cells of eight times the unit cell volume.

Modeling of HoAgGe crystal using direct minimization of the Potts Hamiltonian

Supplemental materials

I. MAGNETIC STATES

The specific magnetic states found using the RCS Search method for the HoAgGe crystal are shown below in Figs. 1 - 13. The average magnetization of the Ho atoms (normalized to the saturation field for $\mathbf{h}||x$ and $\mathbf{h}||y$ respectively) and the Magnetic Space Group (MSG) are listed as well. It should be noted that several of these states are not unique and characterize a family of symmetrically equivalent states. For example, there are 6 equivalent ground states representable on the $\sqrt{3} \times \sqrt{3}$ Magnetic Unit Cell. This number of equivalent states only increases with the consideration of differently shaped cells. However, as described in the main text, only one state actually needs to be considered.

A. States found for magnetic fields applied in the X direction

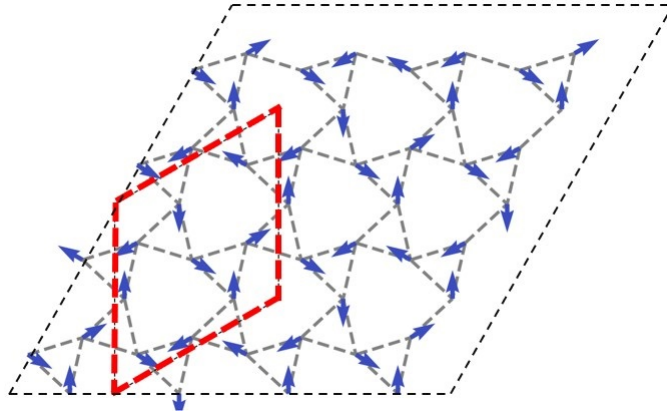


FIG. 1: The ground ($\langle M \rangle_x = 0$) magnetic state for the Ho crystal. (MSG: $P\bar{6}'m2'$)

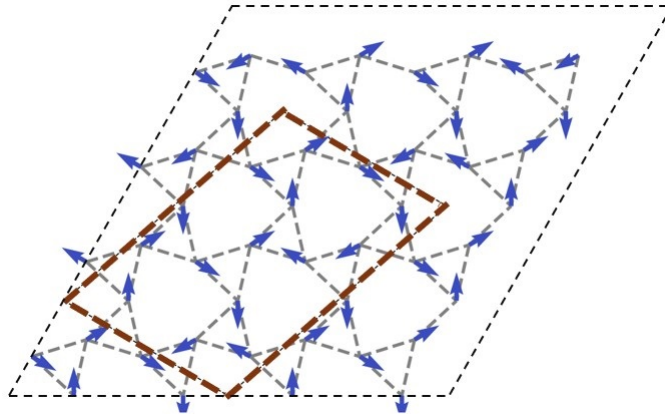


FIG. 2: The $\langle M \rangle_x = 1/5$ magnetic state for the Ho crystal. (MSG: $Am'm2'$)

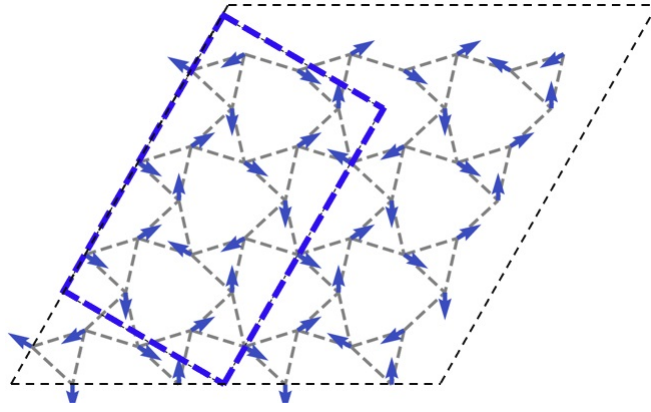


FIG. 3: The $\langle M \rangle_x = 1/3$ magnetic state for the Ho crystal. (MSG: Pm')

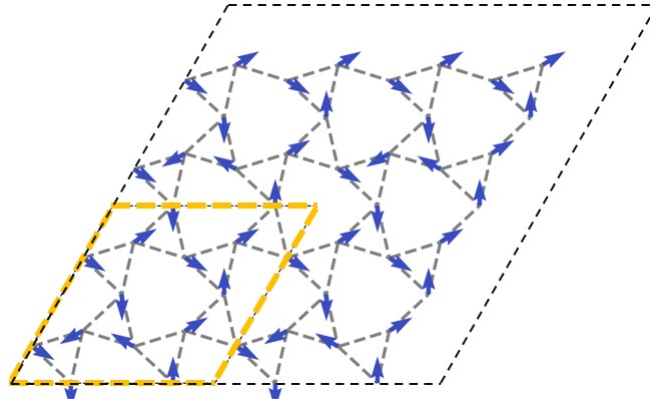


FIG. 4: The $\langle M \rangle_x = 1/2$ magnetic state for the Ho crystal. (MSG: Pm')

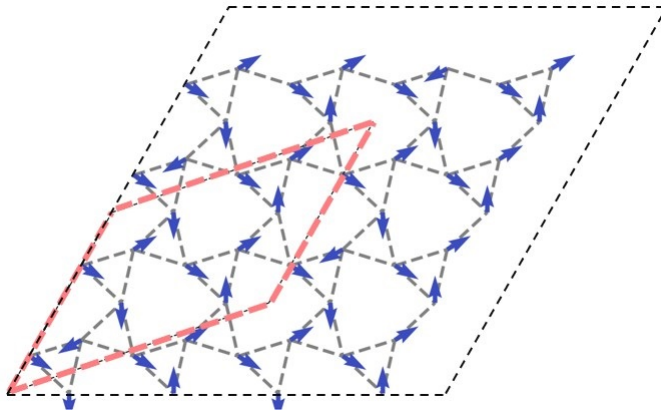


FIG. 5: The $\langle M \rangle_x = 3/4$ magnetic state for the Ho crystal. (MSG: Pm')

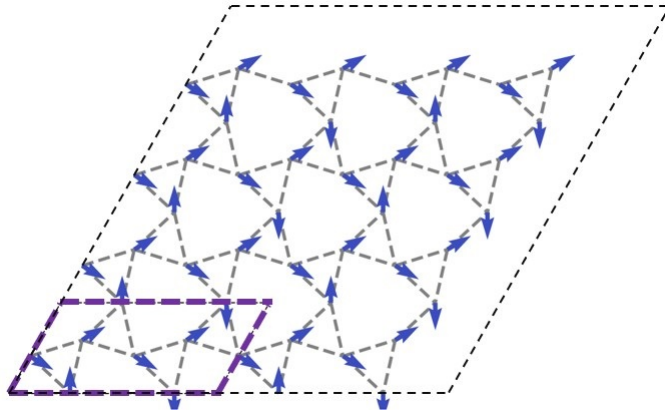


FIG. 6: The saturated ($\langle M \rangle_x = 1/1$) magnetic state for the Ho crystal. (MSG: Pm')

B. States found for magnetic fields applied in the Y direction

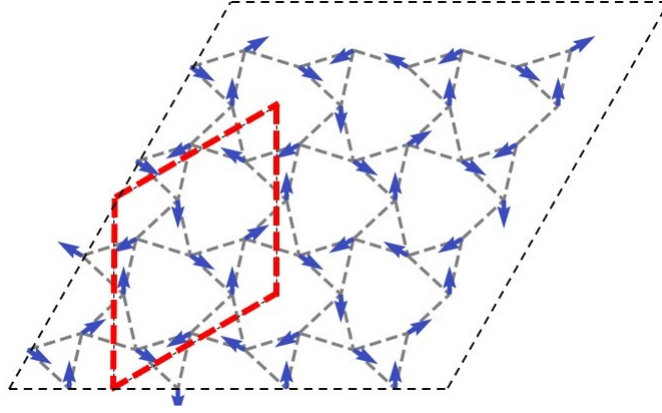


FIG. 7: The ground ($\langle M \rangle_y = 0$) magnetic state for the Ho crystal. (MSG: $P\bar{6}'m2'$)

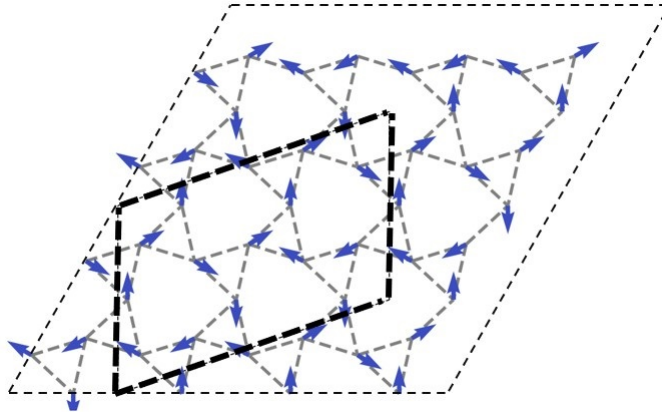


FIG. 8: The $\langle M \rangle_y = 1/5$ magnetic state for the Ho crystal. (MSG: $Am'm2'$)

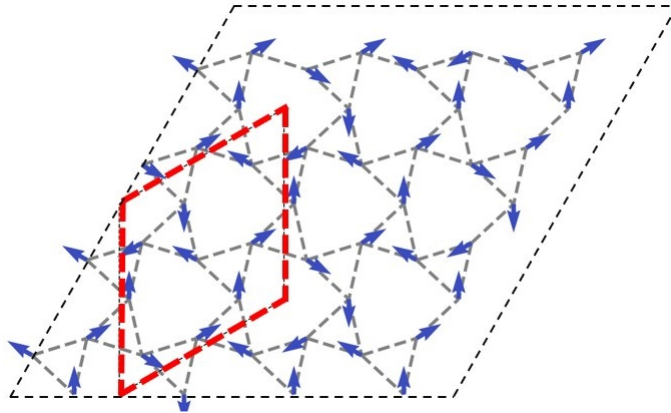


FIG. 9: The $\langle M \rangle_y = 1/3$ magnetic state for the Ho crystal. (MSG: $Am'm2'$)

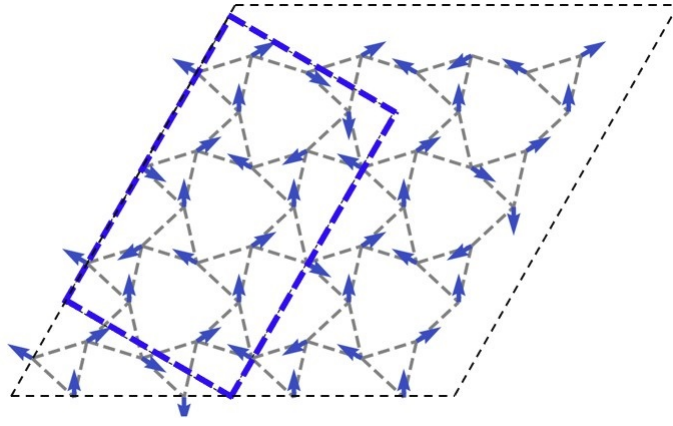


FIG. 10: The $\langle M \rangle_y = 1/2$ magnetic state for the Ho crystal. (MSG: Pm')

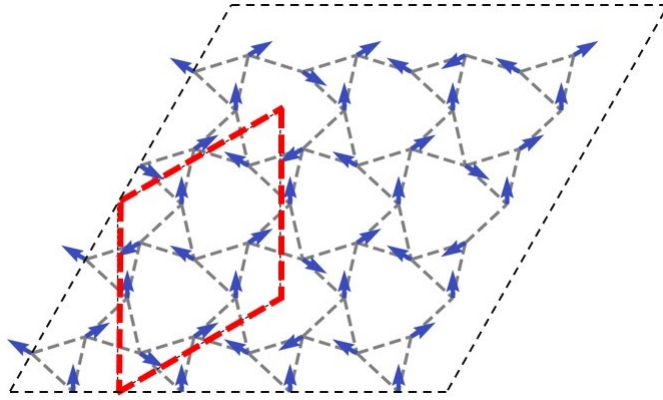


FIG. 11: The $\langle M \rangle_y = 2/3$ magnetic state for the Ho crystal. (MSG: Am'm2')

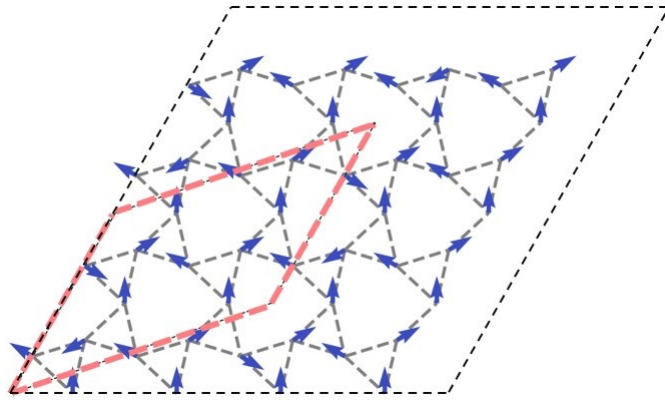


FIG. 12: The $\langle M \rangle_y = 3/4$ magnetic state for the Ho crystal. (MSG: Pm')

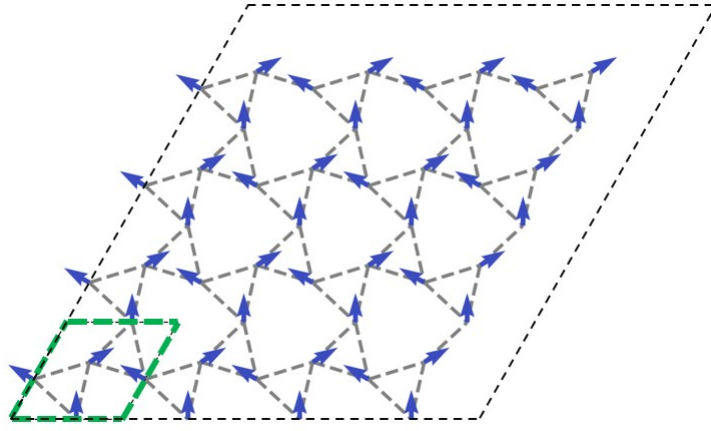


FIG. 13: The saturated ($\langle M \rangle_y = 1/1$) magnetic state for the Ho crystal. (MSG: Am'm2')

II. PHASE DIAGRAMS

The complete $J_\alpha - h$ magnetic and state phase diagrams are shown below. These were again found using an RCS Search method.

A. Magnetic Phase Diagrams

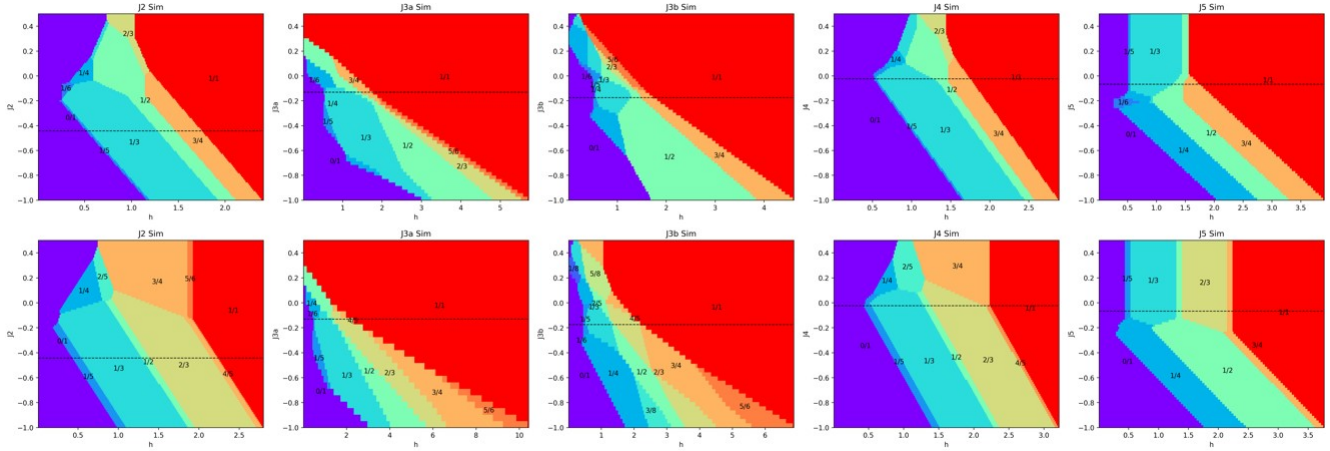


FIG. 14: Average magnetization phase diagrams for bond parameters $J_2, J_{3a}, J_{3b}, J_4, J_5$ for a magnetic field applied in the X (top) and Y (bottom) directions. Dotted line indicating the theorized value for J_α

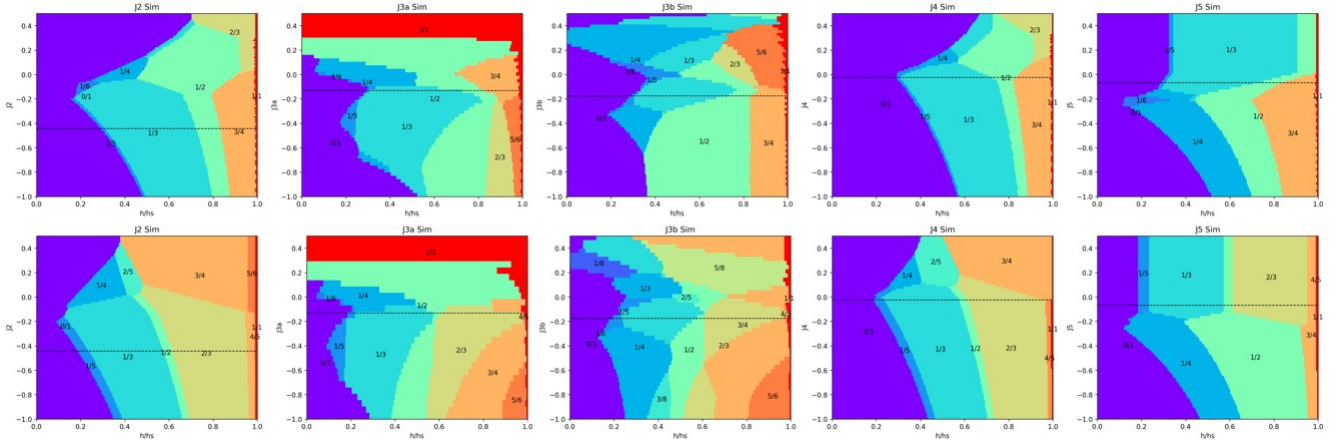


FIG. 15: Average magnetization phase diagrams for bond parameters $J_2, J_{3a}, J_{3b}, J_4, J_5$ for a magnetic field applied in the X (top) and Y (bottom) directions, normalized to saturation field. Dotted line indicating the theorized value for J_α

B. State Phase Diagrams

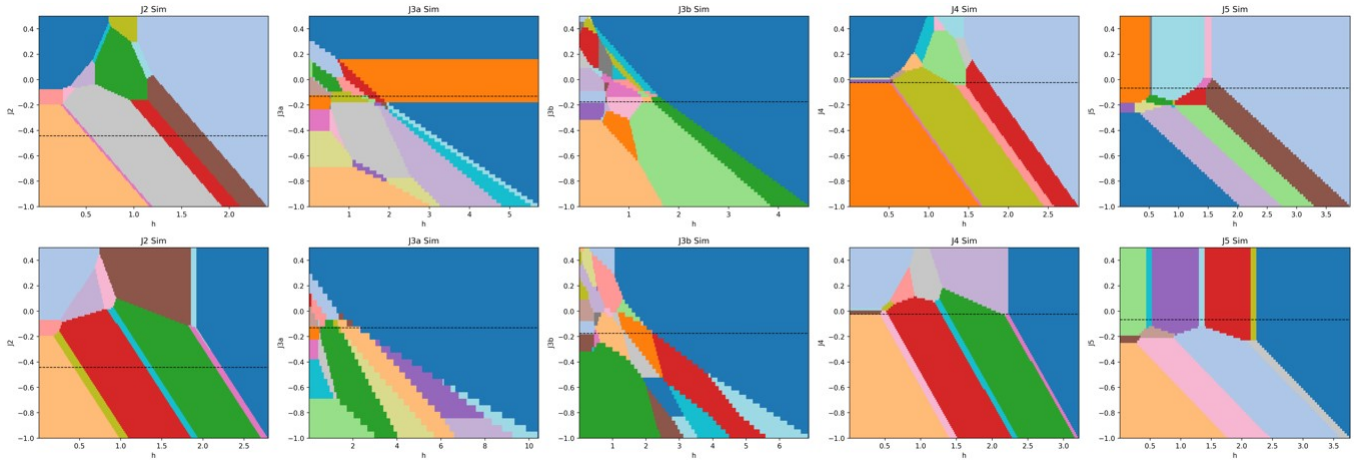


FIG. 16: Magnetic state phase diagrams for bond parameters $J_2, J_{3a}, J_{3b}, J_4, J_5$ for a magnetic field applied in the X (top) and Y (bottom) directions. Dotted line indicating the theorized value for J_α

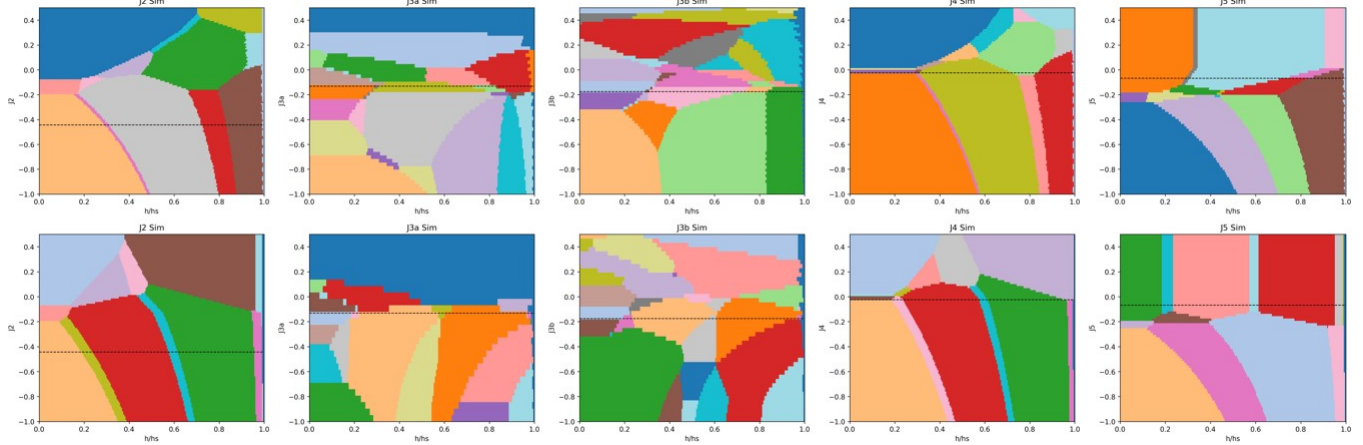


FIG. 17: Magnetic state phase diagrams for bond parameters $J_2, J_{3a}, J_{3b}, J_4, J_5$ for a magnetic field applied in the X (top) and Y (bottom) directions, normalized to saturation field. Dotted line indicating the theorized value for J_α

III. ENERGY VS APPLIED FIELD

Average energy per Ho atom can be plotted for each Magnetic Unit Cell considered. Below we can see the close competition between all 27 acceptable Magnetic Unit Cells with volume less than or equal to 6 times the Unit Cell volume. As described earlier, only the minimum energy state will be observed, meaning only the state corresponding to the bottom most line.

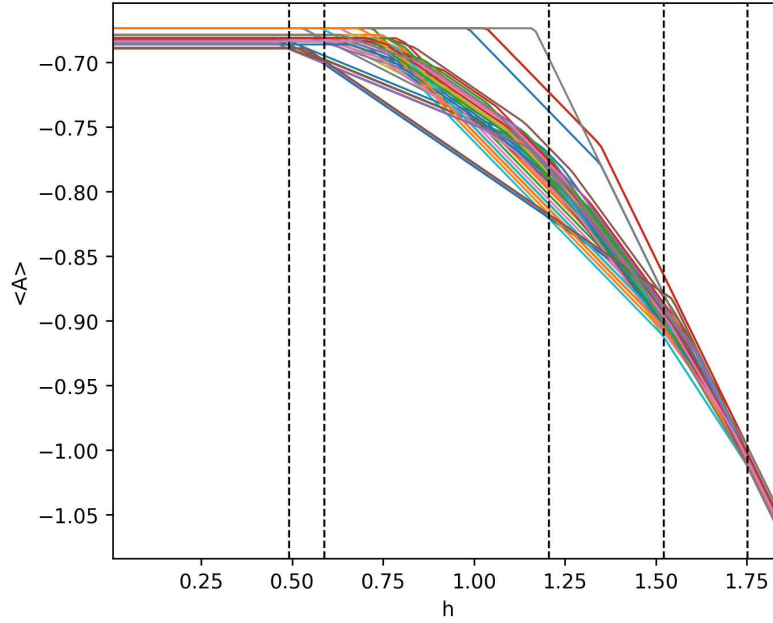


FIG. 18: Minimum average energy per Ho atom ($\langle A \rangle$) of different Magnetic Unit Cell guesses as external magnetic field ($h||x$) is applied. (Vertical dotted lines indicating phase transitions)

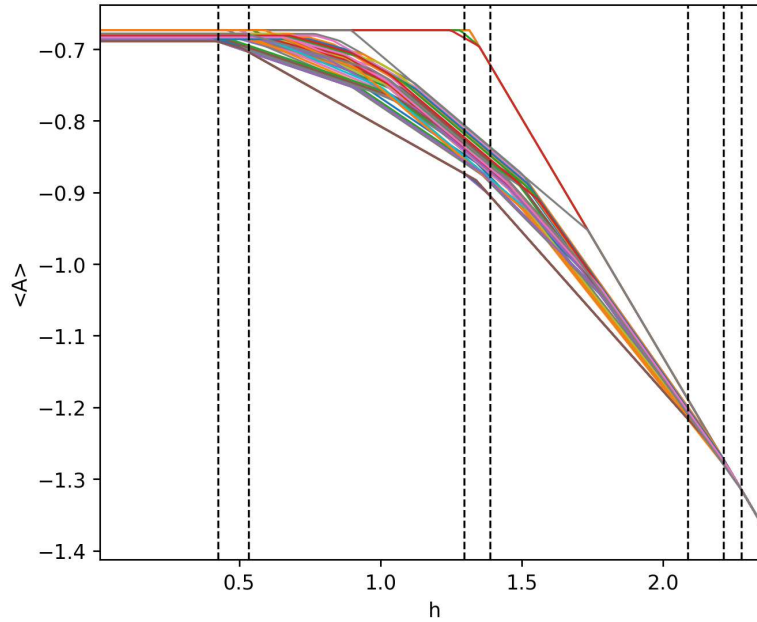


FIG. 19: Minimum average energy per Ho atom ($\langle A \rangle$) of different Magnetic Unit Cell guesses as external magnetic field ($h||y$) is applied. (Vertical dotted lines indicating phase transitions)